15th IFK
Proc. of the 15th International Fluid Power Conference <Symposium/Conference>
<DOI>

Modelling and Simulation of Damping Orifices for Pressure Control Valves (2nd Report)

Seiei Masuda*, Yasushi Matsunaga*, Fumio Shimizu, Kazuhiro Tanaka****

*IHI Corporation, Control Systems Engineering Department, 3-2-1 Daikanyama, Akishima City, Tokyo, Japan**

*Kyushu Institute of Technology, Graduate School of Computer Science and Systems Engineering, 680-4 Kawazu, Iizuka-shi, Fukuoka, JAPAN***

masuda4361@ihi-g.com, matsunaga4536@ihi-g.com, shimizu@phys.kyutech.ac.jp, tanakafa@fka.att.ne.jp

Abstract.

Because alternating flow passes through the damping orifice in a pressure control valve, the size and location of the contraction region are not well understood. However, it is known that the flow coefficient of the orifice is significantly affected by the contraction coefficient of the jet. If the flow coefficient of the damping orifice fluctuates depending on the frequency of the alternating flow, a 40% change in the flow coefficient poses a risk of a 6 dB increase or decrease in the gain margin of the pressure control system. This research was motivated by this risk, predicted from a 1D model of the pressure control valve. There is a high need to reduce the risk to stability of the pressure control system inside an aircraft jet engine fuel control device, whose operating range varies significantly depending on flight conditions. The authors previously presented the above risk in reference [1]. When considering the dynamic characteristics of an orifice, they approximate it as an LRC circuit. In this case, L in the LRC circuit is corrected for the fluid inertia of the short choke tube, and the R element can be approximated as the orifice opening area, and the C element can be approximated as the fluid compressibility upstream of the orifice. Comparison with CFD frequency response demonstrated its validity. The remaining issues include the effect of the damping orifice delay on the differential pressure control valve, understanding the effect of the damping orifice amplitude, deriving the correction value for the *L* element, and confirming the flow pattern that the alternating flow has on the orifice. This paper reports on the progress of the results of these investigations and also mentions the remaining issues.

Keywords. Pressure Control Valve, Damping Orifice, Alternative Flow, Flow Pattern, Flow Coefficient, Bond graph, LRC Circuit, Frequency Response Diagram, CFD

1. INTRODUCTION

Most jet engine fuel metering units today combine a fuel metering valve, which can control the metering port opening area to a desired value through feedback control using a digital controller, with a differential pressure control valve, a type of pressure control valve, which maintains a constant differential pressure across the fuel metering valve. Because the flow velocity of the fuel metering valve is proportional to the square root of the differential pressure and regulated to constant, the fuel metering flow is proportional to the metering port opening area.[11][12] As noted in [1], the differential pressure control valves, which is a type of pressure control valve used in the fuel control units of aircraft jet engines must achieve both stability and responsiveness over a wide operating range. Among these valves, the dynamic characteristics of the differential pressure control valve, which maintains a constant differential pressure across the fuel metering valve, are particularly important because they directly affect the stability of the fuel flow rate itself. On the other hand, pressure disturbances are directly applied to the differential pressure across the metering valve; however, the control of the metering valve opening area is performed by feedback control. By designing the bandwidth of the fuel metering valve to be low, the system becomes robust against high-frequency disturbances, and the effects of pressure disturbances can be more easily compensated by the feedback control. The configuration of a differential pressure control valve is shown in Figure 1.

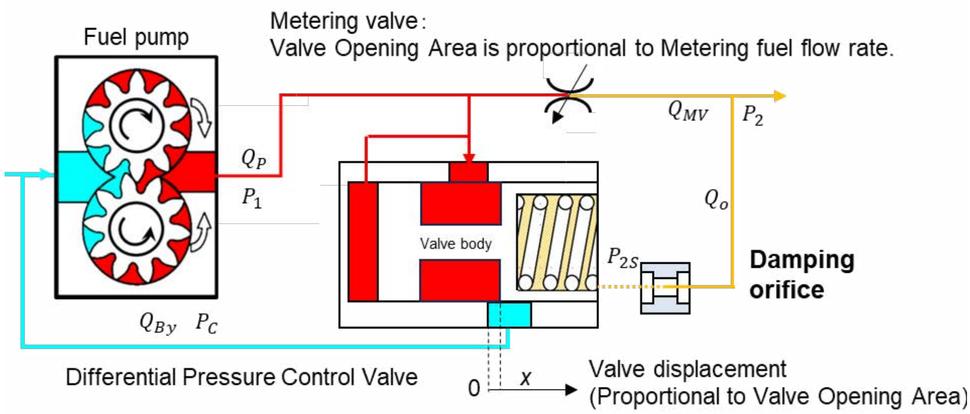

Figure 1 Schematic Diagram of a Pressure Control Valve [1]

Typically, the differential pressure sensing valve operates by multiplying the differential pressure between the control pressure and the reference pressure by the valve's pressure-receiving area to generate a fluid force. This force balances against a preloaded spring force to determine the valve's position. Additionally, a reaction force from the valve's damping resistance is applied, imparting dynamic characteristics to the spring-mass system. Differential pressure control valves must respond sufficiently quickly to changes in fuel flow and maintain adequate stability margin across the entire operating range. This prevents unexpected fuel flow overshoot. To achieve this, the damping ratio of the valve body's spring-mass system is increased beyond the limit damping ratio using a damping orifice, reducing the rate of change of phase margin with frequency. The proportional gain is set so that the crossover frequency satisfies the lower limit of the responsiveness requirement, while ensuring sufficient stability margin is always maintained under the valve spool geometry and operating conditions.

In the pressure control valve's spring-mass system, a damping orifice is placed in series with the valve spool and is used to provide damping force ideally proportional to valve velocity. Typically, the damping force exhibits a characteristic proportional to the square of the flow rate through the orifice, resulting in zero damping force at valve standstill and significant nonlinearity. [2] [6] [7] In the damping orifice, the flow pattern through the orifice, such as the direction of flow rotation, is considered to exhibit symmetry in both positive and negative directions. Furthermore, the effect of changes in flow pattern on the orifice's Pena-Contractor section is expected to vary significantly with frequency.

However, there are few studies on the frequency response, flow pattern, contraction coefficient, and flow coefficient of the damping orifice in hydraulic pressure control valves. Oshima et al. [2] and Miyashita [3] reported experimental results on the frequency response of damping orifices, but did not mention flow patterns. Furthermore, research on pulsating flow by Nakano et al. [4] has been conducted, sharing many commonalities from a modelling perspective. However, in alternating flow, the average flow velocity is zero. Since the damping force has polarity and is proportional to the square of the flow velocity, the damping force becomes zero in the valve's steady state and varies significantly with velocity amplitude. If the damping force were zero, the valve's spring-mass system would not be damped and would continue oscillating at a constant amplitude. When the valve vibrates, the damping force acts, reducing the amplitude. A method to estimate the valve amplitude in this state has not yet been established.

On the other hand, Iimura et al. [10] studied the equivalent electrical circuit model and transfer function of the Pitot tube orifice in air pressure control applications. The Pitot tube is a type of air speed indicator and a pressure measurement device, so its input is pressure and its output is pressure. While similarities exist in the shape of the transfer function and other aspects, differences between aircraft and liquid systems, as well as the disparity between pressure and flow rate as inputs, necessitate an evaluation of this similarity.

2. PURPOSE

This study reports on further investigations into the results obtained by modelling the frequency characteristics of the damping orifice in a pressure control valve using unsteady CFD analysis and a Bond graph model, aiming to clarify the dynamic characteristics of the damping orifice. Specifically, it reports on the effect of damping orifice delay on differential pressure control valves, understanding the influence of damping orifice amplitude, deriving correction values for L-elements, and confirming flow patterns affecting orifices in alternating flow.

3. 1D MODELLING AND SIMULATION

3.1. *Equations of the Pressure Control valve and the Damping orifice*

We derive the linearized transfer function of the differential pressure control valve receiving flow from the flow source. The derivation of the differential pressure control valve transfer function below is based on Reference [5][6][7][8]. Furthermore, regarding the dynamic characteristics of the damping orifice, we add the differential pressure caused by fluid inertia occurring in the short pipe section of the orifice restriction, as described in Reference [1]. The objective is to verify changes in crossover frequency and phase margin in response to variations in the damping force or damping ratio within the differential pressure control valve. However, the purpose of this paper is to outline the impact of changes in the damping orifice on the entire differential pressure control system. NOMENCLATURE lists the symbols used in deriving the transfer function.

Equation (3.1) shows the equilibrium of forces acting on the valve body of a differential pressure control valve. For simplification, the fluid viscous resistance and friction force of the spool valve are approximated as zero, and the viscous resistance is only the damping force from the damping orifice. Similarly, the fluid force is also assumed to be negligible. These simplifications do not compromise the generality for high-precision spool valves. The motion equation of the valve body is balanced by the fluid dynamic force due to the differential pressure acting on the valve's pressure-receiving area and the spring force. Here, x denotes the valve displacement of the differential pressure control valve, M is the mass of the spool valve, C is the viscous resistance coefficient, k is the spring constant of the pressure control valve, A_R is the receiving area of the spool, P_1 is the pressure upstream of the pressure control valve, and P_2 is the pressure downstream of the metering valve.

$$M \cdot \ddot{x} + C \cdot \dot{x} + k \cdot x = A_R \cdot (P_1 - P_2) \qquad (3.1)$$

The damping force generated by the damping orifice of the differential pressure control valve is expressed by equation (3.2). Here, P_{2s} is the pressure in the spring chamber obtained from P_2 after passing through the damping orifice.

$$F_o = A_R \cdot (P_{2s} - P_2) \qquad (3.2)$$

The damping orifice is modelled below. The differential pressure across the damping orifice is defined by equation (3.3). Here, P_O is the differential pressure of the damping orifice, and PL is the pressure due to fluid inertia as it passes through the short pipe section of the damping orifice. In addition to the pressure loss due to the orifice restriction, the pressure changes originating from the inertial force generated in the short pipe section of the restriction is also formulated. The pressure downstream of the metering valve is governed by the dynamic characteristics of the jet engine and changes sufficiently slowly, so its time variation can be considered negligible, resulting in equation (3.4).

$$P_{2s} - P_O - PL = P_2 \qquad (3.3)$$

$$\frac{d}{dt} P_2 \cong 0 \qquad (3.4)$$

The relationship between flow rate and pressure loss for the damping orifice is shown in Equation (3.5). Here, ρ represents the fluid density, Q_o represents the flow rate through the orifice, A_o represents the orifice opening area, and C_d represents Coefficient of discharge flow r*ate* of the orifice.

$$P_O = \frac{\rho}{2} \left(\frac{Q_O}{C_d \cdot A_o} \right)^2 \qquad (3.5)$$

Fluid inertia is shown in Equations (3.6) and (3.7). This paper considers the pressure due to the inertial effect occurring in the short pipe of the orifice.[6] [7] Here, L represents the length of the pipe of the damping orifice.

$$PL = IL \frac{d}{dt} Q_o \qquad (3.6)$$

$$IL = \frac{\rho \cdot L}{A_o} \qquad (3.7)$$

Equation (3.8) represents the flow rate applied to the damping orifice from the differential pressure control valve.

$$Q_{In} = A_R \cdot \dot{x} \qquad (3.8)$$

Substituting the equations for each element into equation (3.3) yields equation (3.9). Linearizing equation (3.9) results in equations (3.10) and (3.11).

$$P_{2s} = \frac{\rho}{2}\left(\frac{Q_O}{C_d \cdot A_O}\right)^2 + IL \cdot \frac{d}{dt} Q_O \qquad (3.9)$$

$$\Delta P_{2s} = R \cdot \Delta Q_O + IL \cdot \frac{d}{dt} \Delta Q_O \qquad (3.10)$$

$$= \rho \frac{(\Delta P_O)_0}{(Q_O)_0} \qquad (3.11)$$

The upstream pressure at the dumping orifice is calculated by integrating the difference between the inflow rate and the flow rate through the orifice using Equation (3.8), as given by Equation (3.12). [6] [7] B represents Bulk modulus of fluid. V_s represents the volume upstream of Spring room. Here, Equation (3.13) represents the spring effect of the hydraulic pressure.

$$P_{2S} = \int \frac{B}{V_s} (A_R \cdot \dot{x} - Q_O) dt + P_{2S0} \qquad (3.12)$$

$$C_I = \frac{B}{V_s} \qquad (3.13)$$

Taking the Laplace transform of equation (3.12) and substituting equation (3.8) yields equation (3.14). Here, Δ indicates a prefix of variable for micro-time perturbation and C_I represents the *C* element of damping orifice Volume. And *s* represents Laplace operator. Q_{In} represents the input flow rate of damping orifice.

$$\Delta P_{2S} = \frac{1}{s} C_I (Q_{In} - Q_O) \qquad (3.14)$$

Substituting equation (3.9) into equation (3.14) gives the relationship between Q_{In} and Q_o as equation (3.15).

$$\frac{\rho}{2}\left(\frac{Q_O}{C_d \cdot A_O}\right)^2 + IL \cdot \frac{d}{dt} Q_O = \frac{1}{s} \cdot C_I \cdot (Q_{In} - Q_O) \qquad (3.15)$$

The transfer function from linearized Q_{In} to Q_o is derived from equations (3.16) to (3.17). Here, *R* represents the R element of orifice restriction.

$$R \cdot \Delta Q_O + IL \cdot \frac{d}{dt} \Delta Q_O = \frac{1}{s} \cdot C_I \cdot (\Delta Q_{In} - \Delta Q_O) \qquad (3.16)$$

$$Q_O = \frac{C_I}{IL \cdot s^2 + R \cdot s + \cdot C_I} Q_{In} \qquad (3.17)$$

$$\Delta P_{2s} = \frac{C_I \cdot (R + IL \cdot s)}{IL \cdot s^2 + R \cdot s + \cdot C_I} Q_{In} \tag{3.18}$$

Furthermore, from equations (3.1) and (3.8), the damping coefficient C is obtained as shown in equation (3.19). Since the characteristics of the damping orifice vary significantly with amplitude, applying a sinusoidal frequency sweep input to the nonlinear state equations and performing a Fourier transform on the input and output yields a transfer function nearly equivalent to a linear transfer function. That is, equation (3.20) shows the second-order nonlinear state equation. By applying a frequency-swept input to Q_{In} while varying the amplitude, the frequency response curve for each amplitude can be obtained.

$$C \cdot \dot{x} = A_R \cdot \Delta P_{2s} = \frac{{A_R}^2 \cdot C_I \cdot (R + IL \cdot s)}{IL \cdot s^2 + R \cdot s + \cdot C_I} \dot{x} \tag{3.19}$$

$$\begin{bmatrix} \dot{P_{2s}} \\ Q_O \end{bmatrix} = \begin{bmatrix} C_I(Q_{In} - Q_O) \\ \frac{1}{IL}\left(\Delta P_{2s} - \frac{\rho}{2}\left(\frac{Q_O}{C_d \cdot A_o}\right)^2\right) \end{bmatrix} \tag{3.20}$$

In the motion equation of the valve body for a pressure control valve, damping resistance is dominated by the damping orifice. For precision valves, friction and fluid viscous resistance can be considered negligible. The control pressure for a differential pressure control valve varies due to the compressibility of the fluid and the bypass flow rate of the differential pressure control valve. Equation (3.21) relates the upstream pressure of a differential pressure control valve to the inflow rate into its volume. Here V represents the volume upstream of metering valve. Q_P, Q_{By} *and* Q_{MV} represent the input flow rate of damping orifice, the metering fuel flow rate and the flow source discharge flow rate.

$$P_1 = \int \frac{B}{V} \left(Q_P - Q_{By} - Q_{MV}\right)dt + P_{10}) \tag{3.21}$$

Equation (3.22) relates the orifice area of a pressure control valve to its flow rate based on Bernoulli's law. [6][7] Here A_{By} represents Pressure control valve opening area. k_V represents the pressure control valve opening area per displacement.

$$Q_{By} = C_d \cdot A_{By} \sqrt{\frac{2 \cdot (P_1 - P_c)}{\rho}} = C_d \cdot k_V \cdot x \sqrt{\frac{2 \cdot (P_1 - P_c)}{\rho}} \tag{3.22}$$

Equation (3.23) shows the linearized transfer function between the upstream pressure of a differential pressure control valve and its bypass valve orifice area.

$$\Delta P_1 = \frac{-2 \cdot (P_1 - P_c)_0}{Q_P} \cdot \left(\frac{Q_{By}}{A_{By}}\right)_0 \cdot \frac{1}{1 + \frac{V}{B} \cdot \frac{2 \cdot (P_1 - P_c)_0}{Q_P} s} \cdot k_V \cdot \Delta x \tag{3.23}$$

Figure 3.1 shows a block diagram of the overall linearized transfer function of the differential pressure control valve. In the open-loop transfer function depicted in this block diagram, the crossover frequency and the phase delay at that frequency can be used as evaluation metrics for responsiveness and stability. By satisfying each required value, it is possible to determine whether responsiveness and stability can be achieved simultaneously.

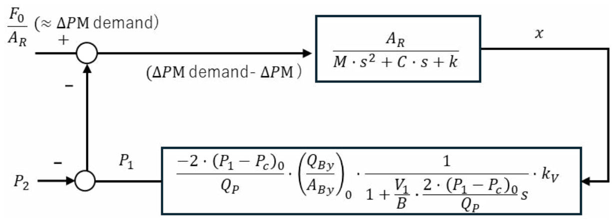

Figure 3.1 Block Diagram of Differential Pressure Control Valve

3.2. Frequency Response Results for Damping Orifice

Frequency response simulations were performed using a sinusoidal frequency sweep input to vary the amplitude in the state equation for the damped orifice (Equation 3.20). Frequency Response Simulation Conditions is shown Table 3.1. Figure 3.2 shows the time series of the waveform of a sinusoidal sweep of the orifice input flow rate. The input waveform is the same, but the flow rate amplitude is different. Figure 3.3 shows the time series response of the normalized orifice differential pressure. Figure 3.4 also shows the normalized response when the internal inertance of the orifice is changed. Each frequency response diagram is shown in Figures 3.5 and 3.6. When the input amplitude and the response is small, as shown in Figure 3.3 a) or b), the amplitude increases with frequency relative to the input, exhibiting a peak frequency. However, as the input amplitude increases, as seen in Figure 3.3, the peak amplitude tends to decrease. The frequency response diagrams with varying amplitude in Figure 3.5 show a first order/second-order response at small amplitudes. As the amplitude increases, the open-loop gain of the orifice's LCR circuit decreases, phase margin increases, and the response approaches a first-order lag shape. For the short pipe section of the orifice, it was confirmed that the frequency changes with pipe length, like the linear analysis.[1]
In addition, Figure 3.6 shows the change in the Bode diagram due to changes in inertance. The results are almost the same as those obtained by Fourier transform analysis. [1]

able 3.1 Frequency Response Simulation Conditions

Simulation Condition	***Dimension***	***Parameter***
Flow Amplitude Range	*mL/min*	a):6.3, b): 31.5, c):63.0, d):314.5, e):630.0
Inertance	*kg/m⁴*	1):1.739E+6, 2):4.288 E+6
Sine Sweep Range	*rad/sec*	From 0.628 to 3000·6.28
Frequency Sweep Time	*s*	0.5
Time Step	*s*	0.5E-06
Integration Method	-	Eulerian Method
ΔP_{2s}	*kPa*	Differential Pressure of orifice

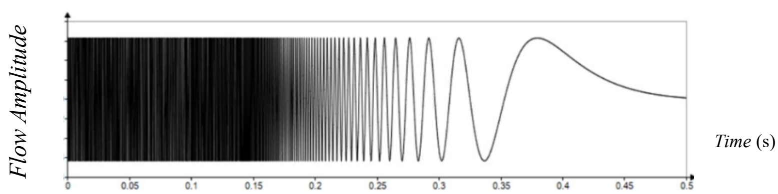

Figure 3.2 Q_{In} sine wave sweep input (from a) to e) have same waveform)

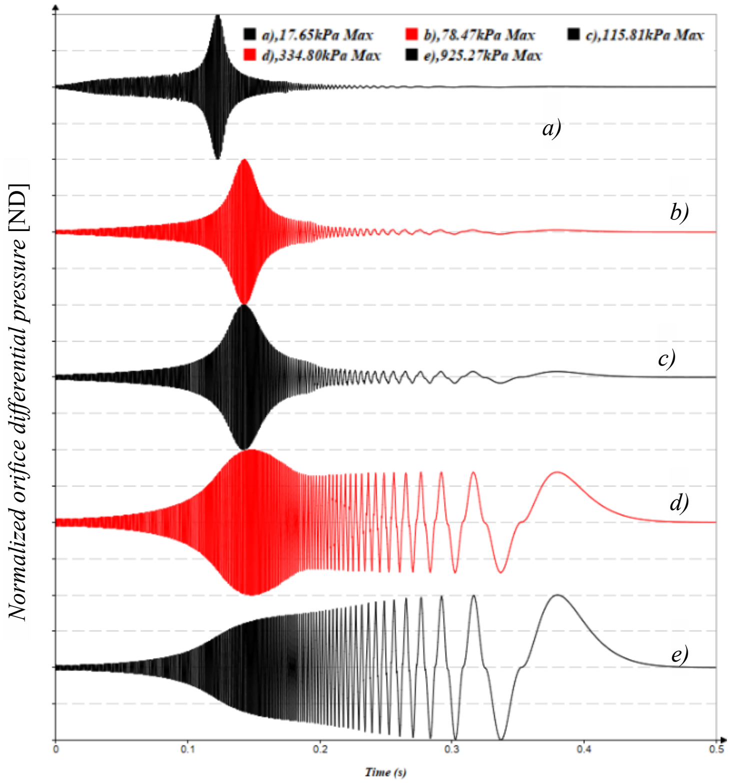

Figure 3.3 Response to Q_{In} input（Normalized ΔP_{2S} Response, Input amplitude change）

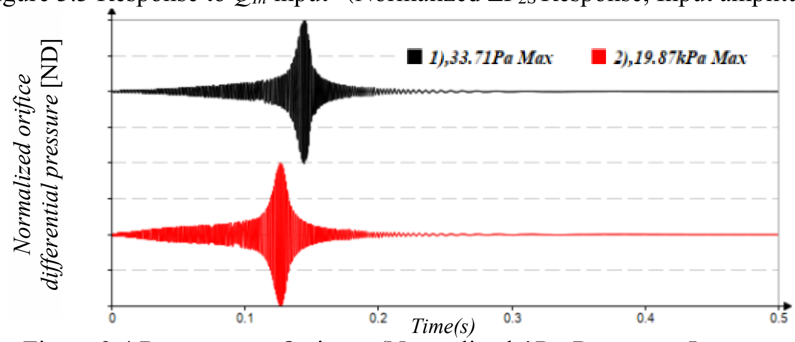

Figure 3.4 Response to Q_{In} input (Normalized ΔP_{2S} Response, Inertance change)

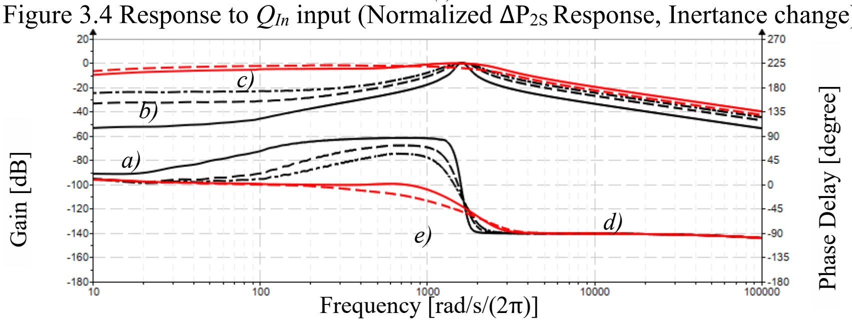

Figure 3.5 Normalized Frequency Response Diagram of $\Delta P_{2S}/ Q_{In}$ (Input amplitude change)

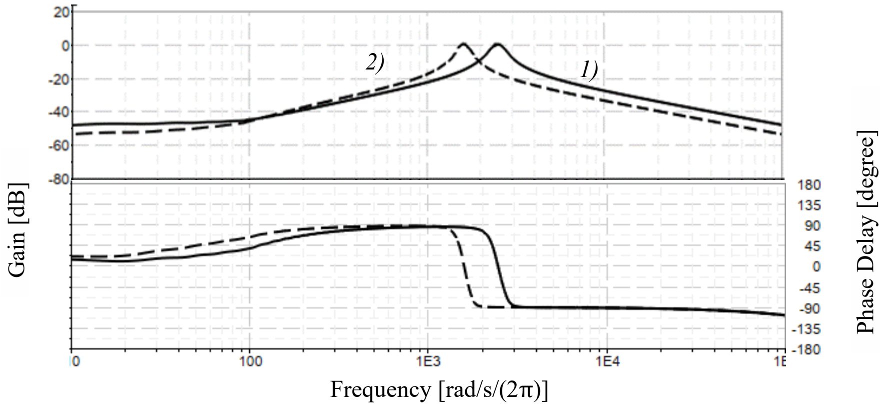

Figure 3.6 Normalized Frequency Response Diagram of $\Delta P_{2S}/\, Q_{In}$ (Input Inertance change)

3.3. Effect of Damping Orifice Transfer Function on the Response of a Differential Pressure Control System

We investigated whether the transfer function of Equation (3.18) affects the frequency response diagram of a differential pressure control system. The transfer function of the damping coefficient in Equation (3.18) was substituted for the damping coefficient in Equation (3.1). Figure 3.7 shows the block diagram before and after the substitution.

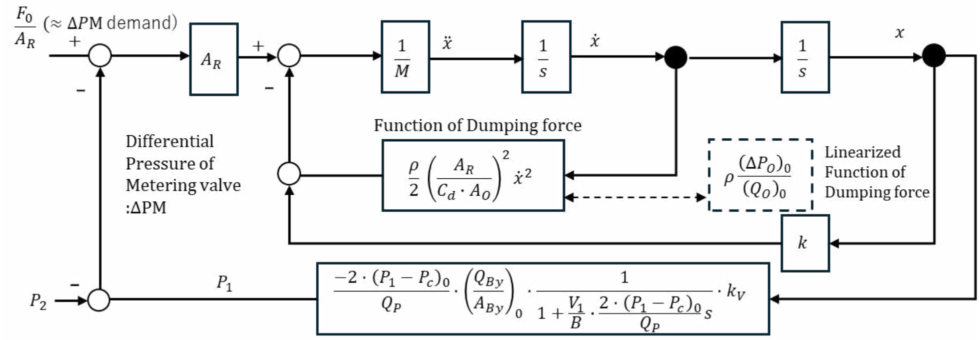

(a) Differential Pressure Control Valve Block Diagram (No Orifice Delay)

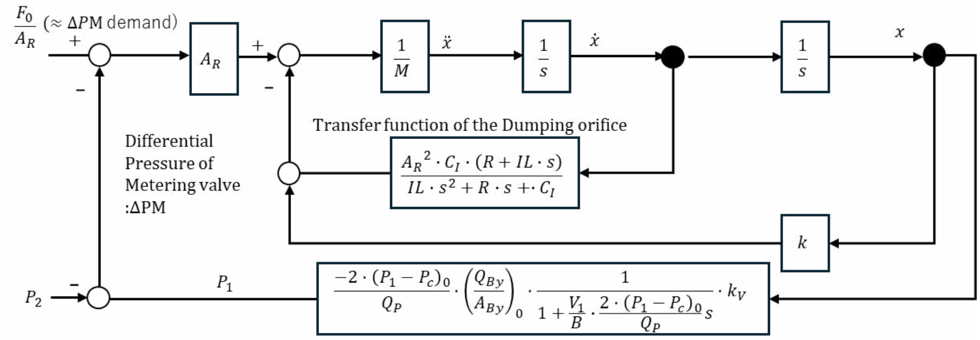

(b) Differential Pressure Control Valve Block Diagram (With Orifice Delay)

Figure 3.7 block diagrams of the Pressure control valve

The transfer function of the pressure control valve with and without orifice delay was calculated by varying the valve amplitude under the conditions listed in Table 3.2. Figure

3.8 shows the Bode diagram. Table 3.2 lists the pressure control valve parameters. The orifice delay has a resonance point at approximately 10000 rad/s (1.6 kHz), which was previously thought to have a small impact due to a frequency band sufficiently different from the bandwidth of the pressure control valve. However, due to factors such as the phase lead element, it can affect the stability and responsiveness of the pressure control valve.

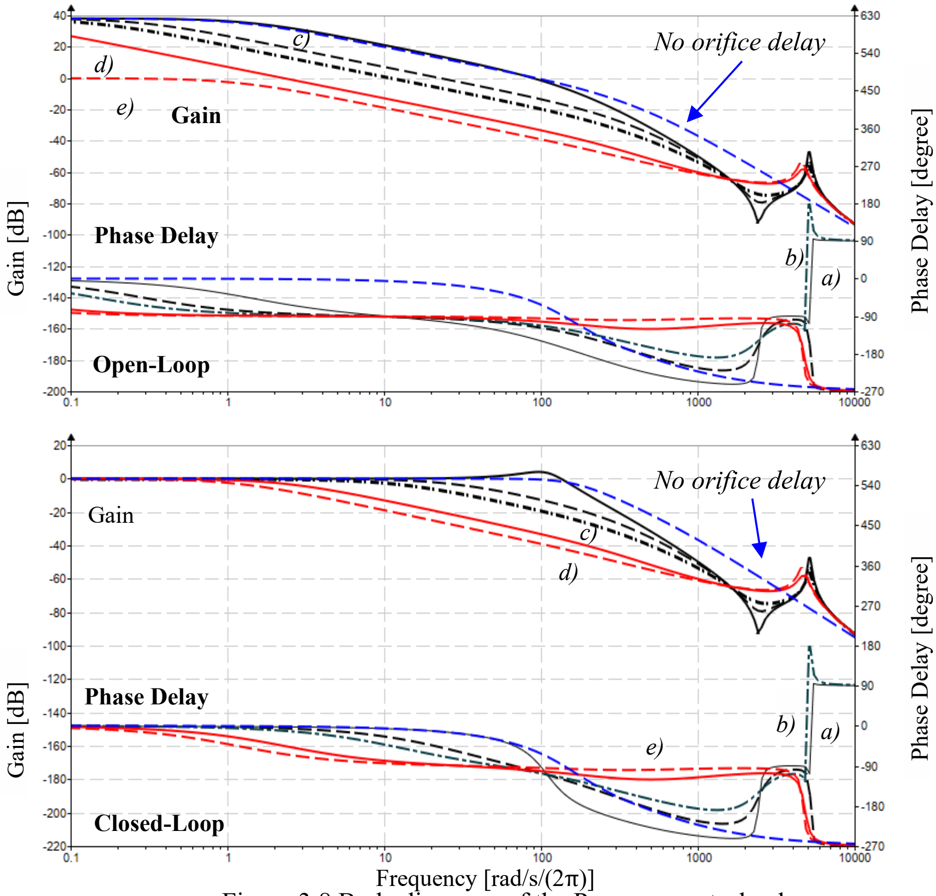

Figure 3.8 Bode diagrams of the Pressure control valve

Table 3.2 Parameter of Pressure Control Valve and simulation conditions

Simulation Condition	***Dimension***	***Parameter***
Inertance of orifice	*kg/m^4*	1.739E+6,
R of orifice	*kg/(s·m4)*	a):1.728e+9, b):8.639E+9, c):1.728E+10, d): 8.639E+10, e): 1.728e+11,
Inertance of orifice	*kg/m^4*	1.739E+6, 2)
C of orifice	*$kg/(s^2 \cdot m4)$*	4.067E+14
Resonant Frequency of The Valve	*rad/sec*	176.14
Mass of Valve	*kg*	0.05
Resistance of Valve	*N/mm/s*	0.2
Open-loop Gain	*ND*	80

It was found that greater stability is achieved when the proportional element or orifice flow rate is large, and resistance: R is high. Because the purpose of this paper is to examine the dynamic characteristics of the orifice, the operating conditions are not yet clear. It was found that even in systems with fast orifice dynamics, the pressure control valve is affected by a frequency band that differs by more than one order of magnitude. A more detailed study will be conducted separately after determining the specifications of the pressure control valve.

4. CFD ANALYSIS

The CFD model used in this study is shown in Figure 4.1. In examining the flow patterns, a simpler orifice model was also considered. However, the unique flow characteristics of the orifice's alternating flow were also reproduced in the model described in [1], so that model is omitted for simplicity's sake. The flow patterns were examined at the timing of changes in flow rate. The 3D model and simulation conditions are shown in Table 4.1, and the simulation model is shown in Figure 4.1. Figure 4.2 shows the velocity diagram near the orifice's short-view and the velocity distribution at the short-view cross section for each simulation. Figure 4.3 also shows the pressure distribution near the orifice. These analyses revealed no contraction within the orifice's short-pipe passage. Furthermore, during the alternating flow transition, a cylindrical flow remained at the orifice exit without changing flow direction, and no fluid flow entered from the orifice's axis when the flow reversed. Therefore, fluid is thought to be entering from the radial direction. Furthermore, the orifice contraction occurs at the orifice entrance and immediately shifts to the opposite side when the flow alternates. Table 4.2 shows the flow coefficient for each orifice frequency at flow amplitude rate:6.3mL/min. Although there is almost no contraction in the flow pattern, the flow coefficient is decreasing. It is thought that the flow rate at the throttle changes because of compressibility and inertia, which is why the flow coefficient changed. However, it is thought that it will be necessary to separate the effects of compressibility and inertia in the future.

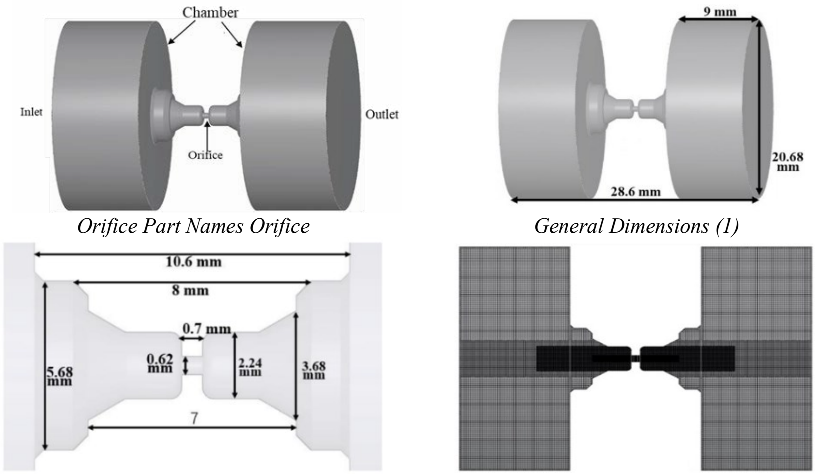

Orifice Part Names Orifice *General Dimensions (1)*

Orifice Detailed Dimensions (2) *Analysis Grid Overview*

Figure 4.1 3D model of CFD Analyses [1]

Table 4.1 Condition of CFD Analyses [1]

Item	Analysis conditions
Software used	Simerics-MP+® [9]
Analysis type	Transient
Turbulence model	Standard k-ε
Fluid density	750 kg/m
Fluid viscosity	9.5×10^{-7} m²/s
Number of grid points	2,488,000
Outlet boundary condition	4.2 MPa
Inlet boundary condition	$Q_{In} = A_R \cdot X \cdot \sin(2\pi \cdot \omega \cdot t)$

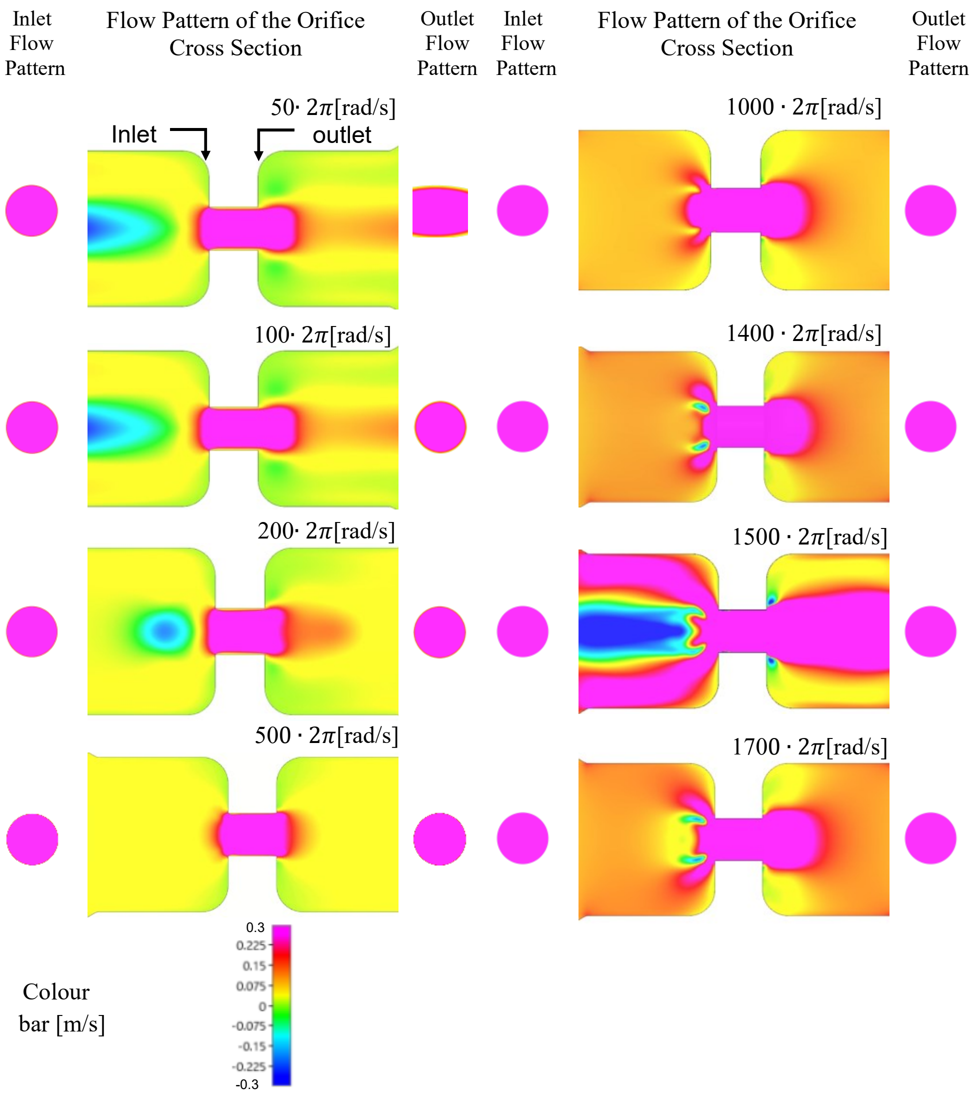

Figure 4.2 Flow patterns of flow velocity near the orifice at each frequency

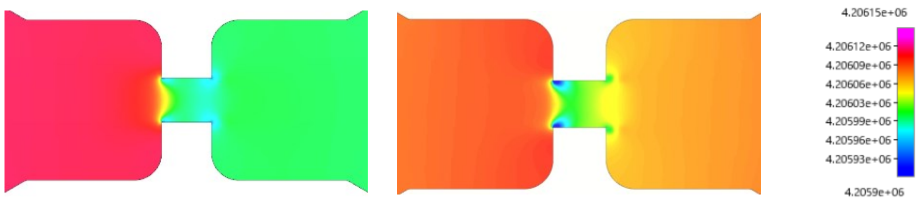

Pressure Distribution at Maximum Flow Rate (500·2π rad/s)   Pressure Distribution at Maximum Flow Rate (1600·2π rad/s)   [Pa]

Figure.4.3 Orifice Pressure Distribution

Table 4.2 flow coefficient of orifices at Flow Amplitude Range:6.3mL/min

Frequency $[rad/s]$	*The flow coefficient*	*Frequency* $[rad/s]$	*The flow coefficient*
50· 2π	0.5	1000· 2π	0.3
100· 2π	0.4	1500· 2π	0.1
200· 2π	0.3	1600· 2π	0.3
500· 2π	0.2	-	-

5. DISCUSSION

5.1. Considerations on the Shift in Orifice Resonance Frequency

In our previous paper, we used transient CFD frequency responses to derive the orifice resonant frequency (the frequency at which the sinusoidal response of the orifice differential pressure to the applied flow rate lags approximately 90 degrees in phase). However, the reason for the approximately 63% decrease in resonant frequency in the 1D modelling was unclear. Based on the flow patterns in the CFD analysis, the inertial length: L, which is proportional to the inertial resistance $\rho \cdot L/A_O$ in the 1D model, appears to be 2.5 times larger in the CFD model. Velocity contours show that a uniform flow from the orifice extends beyond the length of the short pipe. In this paper, we examine the flow patterns and conclude that the increase in inertial length is due to two factors. One factor is additive mass. As shown in [11], when a cylindrical object moves through a fluid, it entrains and simultaneously moves a mass of fluid $3/8 \cdot \rho \cdot (D_O/2)^3$. This increases the inertial length of the fluid by $3 \cdot \pi \cdot D_O/4$. Since D_O=$6 \cdot L/7$ for this orifice, L is expected to be extended by approximately 0.75 times. Furthermore, attachment is expected to occur at both ends of the fluid passing through the short pipe. While additional mass typically occurs at the end face of a spool valve, in this flow, it is expected to attach to the cylindrical fluid in the short pipe. The second factor is that the fluid flow entering and exiting the orifice is similar to the flow field passing through the curtain area of a nozzle/flapper valve, and thus simultaneously moves the cylindrical fluid at the height of the curtain area. Flow along the orifice axis creates a flow pattern that obstructs the flow at both the inlet and outlet of the orifice. Because the flow velocity is slower outside the orifice, the cylindrical flow passing through the orifice continues to flow away from the orifice. When the flow direction is reversed in the orifice's alternating flow, the axial flow near the orifice is obstructed, resulting in radial flow. From a macroscopic perspective, the 90-degree flow bend is like the flow within the curtain area of a nozzle/flapper. This is thought to increase the inertial length, which is equivalent to the curtain area height d/2 (≅3/7L). Figure 5.1 shows a conceptual diagram of inertial length correction around the orifice. Due to the above two factors, the inertial length is thought to increase by approximately 2.2 times. If a shape factor that approximates the radial flow near the orifice to the curtain area can be identified in the future,

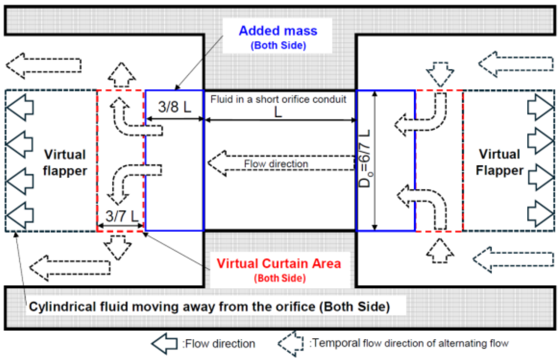

Figure 5.1 Simplified flow pattern near an orifice

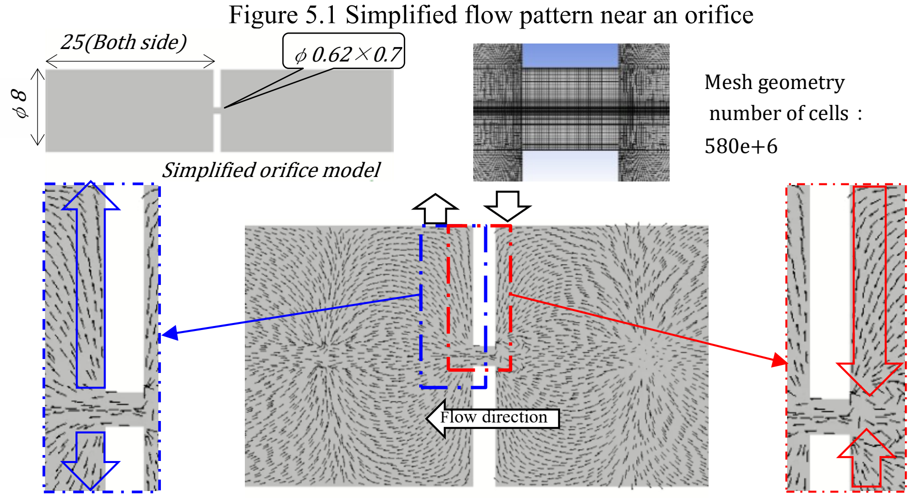

Figure 5.2 Unsteady CFD analysis results for orifice frequency response (vector diagram)

it is expected that the accuracy of deriving the inertial length will improve. Figure 5.2 shows the results of the orifice frequency response analysis using a simplified geometry model with ANSYS CFX, presented as a vector diagram.[13] The frequency is set at $400 \cdot 2\pi[rad/s]$, and the flow rate amplitude is equivalent to that in Table 4.1. ANSYS CFX was used to easily obtain the vector diagrams. As indicated by the arrows in Figure 5.2, the flow pattern on both sides of the orifice exhibits radial inflow (inside of red hollow arrow) and outflow (inside of blue hollow arrow). This flow field is characteristic of the curtain area and occurs just before the direction of the alternating flow changes. It is considered that the radial outflow is generated as the flow from the previous cycle is overtaken and collided with by the flow of the subsequent cycle.

5.2. Considerations on the Shift of the Orifice Natural Vibration

Confirmation of the local discharge coefficient using CFD suggests that no contraction occurs within the orifice. Although contraction does occur before and after the orifice, due to flow symmetry, the location of contraction shifts instantly to the orifice inlet, making the effect of alternating frequency on contraction small. On the other hand, the delay in high frequencies through the orifice is likely to have a significant impact on the flow difficulty. First, we must further investigate whether orifice impedance has any effect on reducing the discharge coefficient. This will require defining the orifice's impedance characteristics using a 1DCAE approach rather than a flow field approach and correlating them with the discharge coefficient as necessary.

6. CONCLUSION

The following was revealed through 1D and 3D orifice simulations.

- In the LCR circuit model of orifice alternating flow, the inertance increased by approximately 2.5 times in the unsteady CFD analysis, and the co-movement frequency decreased by approximately 63%. This is thought to be mainly due to the added mass and the fluid within the curtain area of the virtual nozzle flapper moving simultaneously with the fluid within the pipe. The virtual curtain area is formed by the end face of the added mass, the orifice outlet flow rate, and the surface (virtual flapper) where the axial velocity becomes zero when the flow direction inside the orifice reverses.
- The orifice discharge coefficient is thought to be largely unaffected by the frequency of the alternating flow. Backflow does not occur in short pipes, and the contracted flow that occurs at the orifice inlet quickly moves to the orifice outlet (the inlet after the alternating flow) due to the alternating flow.
- As shown in the example above, the effect of the alternating flow frequency on the discharge coefficient of the steady-state orifice restriction equation is thought to be small. However, the impedance of an LCR circuit is generally affected by the frequency of the alternating flow, and this effect is thought to be dominant.

ACKNOWLEDGMENTS

I would like to express my deep gratitude to Dr. Takeshi Yamaguchi and Ms. Akari Takekawa, a second-year master's student at the Graduate School of Information Engineering, Kyushu Institute of Technology, for their valuable advice on this research.

7. REFERENCES

[1] S. Masuda, Y. Matsunaga, A. Takegawa, F. Shimizu, K. Tanaka, Modelling and simulation of damping orifices for pressure control valves, Proc. ISFP 2024 JFPS, 1A2-03, https://doi.org/10.5739/jfps.52.8

[2] S. Oshima, T. Ichikawa, Frequency Characteristics of Cylindrical Short Chokes for Hydraulic Valves (In case of using general hydraulic oil), J. Hydraul. Pneumatics (Japanese) Vol.15, No.2, 1984, pp.157-165, https://doi.org/10.5739/jfps1970.2.72

[3] S. Miyagawa, Frequency Characteristics of Cylindrical Short Chokes, J. JSME (Japanese) Vol.42, No.355, 1971, pp.847-856, https://doi.org/10.1299/kikai1938.42.847

[4] K. Nakano, S. Yokota, Instantaneous Flowmeter for Hydraulic Systems Utilizing the Dynamic Characteristics of Cylindrical Chokes, J. Hydraul. Pneumatics (Japanese)Vol.17, No.4, 1986, pp.311-317, https://doi.org/10.5739/jfps1970.17.311

[5] S. Masuda, Simulation of the Pressure Control Valve Improving Responsiveness and Stability by Variable Restrict Orifice, Pro. ISFP2017, 2C17

[6] K. Tanaka, Y. Sakurai, System Dynamics and Bondgraphs (2) (Basics of Bondgraph), Turbomachinery Vol.50, No.6, 2022, pp365-375
[7] K. Tanaka, Y. Sakurai, System Dynamics and Bondgraphs (3) (Bondgraph Modelling of Fluid Systems), Turbomachinery Vol.50, No.8, 2022, pp494-505
[8] A. Takegawa, F. Shimizu, S. Masuda, Y. Matsunaga, K. Tanaka, Unsteady Characteristics of Orifice Wake Flow, Proc. JSME Kyushu, Student Conf. 2024
[9] Simerics: Simerics MP+® Manual V5.0 (2019).
[10] I. Iimura, N. Goto, H. Hatanaka, Impedance Characteristics of Orifices, Transactions of the Society of Instrument and Control Engineers, Volume 23 Issue 1 Pages 21-26, 1987
[11] L. C. Jaw, J. D. Mattingly, Aircraft Engine Controls, Aiaa, 2002, pp50-56, https://doi.org/10.2514/4.867057
[12] K. Nishio, M. Endo, Y. Matsuda, The Control of Turbofan Engines, Technical Report of NAL (Japanese), TR-428, 1975, https://jaxa.repo.nii.ac.jp/records/44678
[13] ANSYS: CFX-Pre User's Guide Release 2025R1 (2025)

NOMENCLATURE

Symbol	***Explanation of variable symbols***
A_M	*Metering valve opening area*
C_1	*C element of piping volume*
C_2	*C element of pressure control valve and piping end volume*
D_o	*Diameter of the Dumping orifice*
F_S	*Spring preload*
F_O	*Dumping force of orifice*
F_{DP}	*Force due to differential pressure*
IL	*Inertance of Fluid inertia in orifice pipe*
k_v	*Pressure Control Valve Opening Area per displacement*
t	*Time*
P_{2s}	*Pressure of Spring room*
P_C	*Pressure downstream of Pressure Control valve*
PL	*Effort (pressure) due to fluid inertia*
Po	*Differential pressure of Damping orifice*
R_1	*Pipe pressure loss (pipe resistance) R_1*
R_2	*Pressure control valve restriction R_2*
R_3	*Metering valve restriction R3*
V_1	*Volume upstream of metering valve*
V_S	*Volume upstream of Spring room*
ρ	*Fluid density*
$(X)_0$	*Subscript indicating the steady-state value at time: 0 for variable: X*
ΔPM	*Differential Pressure of Metering Valve*
ΔQ	*Fluid fluctuation in piping volume*
μ	*Viscosity*
ζ	*Damping ratio*

Biographies

Seiei Masuda graduated from the Master course at the Graduate School of Science and Technology, Sophia University, and joined Ishikawajima-Harima Heavy Industries Co., Ltd. (currently IHI Corporation) in 1990. Since then, he has been working in the Mechanical Control Engineering Group, Control Systems Engineering Department, Aerospace and Business Area, mainly developing jet engine fuel control equipment. He holds a Professional Engineer, Japan (Mechanical Engineering), a Professional Engineer, Japan (Engineering Management), and a Doctor of Engineering (Kyushu Institute of Technology, 2020).

Yasushi Matsunaga graduated from the Master's program at the Graduate School of Engineering, Tohoku University in 1986 and joined Ishikawajima-Harima Heavy Industries Co., Ltd. (now IHI Corporation) in the same year. Since then, he has been engaged in research and development of jet engine FADEC systems and rocket turbopumps in the aerospace and business fields.

Fumio Shimizu received his Doctor of Engineering from Tokyo University of Agriculture and Technology in 1995 and subsequently worked in the Department of Physics and Information Technology at the Kyushu Institute of Technology Faculty of Computer Science and Systems Engineering. His research interests include Computational Fluid Dynamics, Gas/Liquid Two-Phase Flow, Acoustic Noise, and Fluid Dynamics.

Kazuhiro Tanaka received his Doctor of Engineering from the University of Tokyo in 1983. He went on to Sophia University and the University of Tokyo and is currently a Professor Emeritus at the Kyushu Institute of Technology.

Research Interests: Thermal/Fluid Engineering, CFD, Fluid Power Systems (Oil-Hydraulics, Pneumatics), Bond Graph Modelling & Simulation